# Neutral sphingomyelinase 2 inhibition attenuates extracellular vesicle release and improves neurobehavioral deficits in murine HIV

**Xiaolei Zhu**[a,b,1],

**Kristen R. Hollinger**[a,1],

**Yiyao Huang**[c],

**Alejandra Borjabad**[d],

**Boe-Hyun Kim**[d],

**Tanina Arab**[c],

**Ajit G. Thomas**[a],

**Mohammed Moniruzzaman**[e],

**Lyndah Lovell**[a],

**Andrey Turchinovich**[f,g],

**Kenneth W. Witwer**[c],

**David J. Volsky**[d],

**Norman J. Haughey**[e],

**Barbara S. Slusher**[a,b,e,h,i,j,k,*]

[a]Johns Hopkins Drug Discovery, Johns Hopkins University School of Medicine, Baltimore, MD, USA

[b]Department of Psychiatry and Behavioral Sciences, Johns Hopkins University School of Medicine, Baltimore, MD, USA

[c]Department of Molecular and Comparative Pathobiology, Johns Hopkins University School of Medicine, Baltimore, MD, USA

[d]Department of Medicine, Infectious Diseases Division, Icahn School of Medicine at Mount Sinai, NY, New York, USA

[*]Corresponding author at: 855 N. Wolfe Street, Rangos 278, Baltimore, MD 21205, USA. bslusher@jhmi.edu (B.S. Slusher).
[1]Co-first authors.

eDepartment of Neurology, Johns Hopkins University School of Medicine, Baltimore, MD, USA

fHeidelberg Biolabs GmbH, Heidelberg, Germany

gDivision of Cancer Genome Research, German Cancer Research Center, Heidelberg, Germany

hDepartment of Medicine, Johns Hopkins University School of Medicine, Baltimore, MD, USA

iDepartment of Neuroscience, Johns Hopkins University School of Medicine, Baltimore, MD, USA

jDepartment of Oncology, Johns Hopkins University School of Medicine, Baltimore, MD, USA

kDepartment of Pharmacology and Molecular Sciences, Johns Hopkins University School of Medicine, Baltimore, MD, USA

## Abstract

People living with HIV (PLH) have significantly higher rates of cognitive impairment (CI) and major depressive disorder (MDD) versus the general population. The enzyme neutral sphingomyelinase 2 (nSMase2) is involved in the biogenesis of ceramide and extracellular vesicles (EVs), both of which are dysregulated in PLH, CI, and MDD. Here we evaluated EcoHIV-infected mice for behavioral abnormalities relevant to depression and cognition deficits, and assessed the behavioral and biochemical effects of nSMase2 inhibition. Mice were infected with EcoHIV and daily treatment with either vehicle or the nSMase2 inhibitor (*R*)-(1-(3-(3,4-dimethoxyphenyl)-2,6-dimethylimidazo[1,2-*b*]pyridazin-8-yl)pyrrolidin-3-yl)-carbamate (PDDC) began 3 weeks post-infection. After 2 weeks of treatment, mice were subjected to behavior tests. EcoHIV-infected mice exhibited behavioral abnormalities relevant to MDD and CI that were reversed by PDDC treatment. EcoHIV infection significantly increased cortical brain nSMase2 activity, resulting in trend changes in sphingomyelin and ceramide levels that were normalized by PDDC treatment. EcoHIV-infected mice also exhibited increased levels of brain-derived EVs and altered microRNA cargo, including miR-183-5p, miR-200c-3p, miR-200b-3p, and miR-429-3p, known to be associated with MDD and CI; all were normalized by PDDC. In conclusion, inhibition of nSMase2 represents a possible new therapeutic strategy for the treatment of HIV-associated CI and MDD.

### Keywords

Neutral sphingomyelinase 2; Depression; Sleep; HIV; Extracellular vesicle; EcoHIV; Mice

## 1. Introduction

The prevalence of major depressive disorder (MDD) is over twice as high in people living with HIV (PLH) as compared to members of the uninfected general population (Ciesla and Roberts, 2001). Comorbid MDD is associated with worse outcomes in PLH, including nonadherence to treatment (Uthman et al., 2014), exacerbated disease progression, and elevated mortality (Anagnostopoulos et al., 2015). Similar to MDD, cognitive impairment (CI) also disproportionally impacts PLH versus the general population and is associated with nonadherence to treatment (Thaler et al., 2015), unemployment (Marquine et al., 2018), and decreased quality of life (Doyle et al., 2012; Tozzi et al., 2003). There is unsurprisingly a

high concordance of CI and MDD in PLH (Shimizu et al., 2011), particularly in cognitive tasks involving information processing speed, verbal learning and memory, attention, and executive function (Fellows et al., 2014).

Extracellular vesicles (EVs) are lipid bilayer-delimited vesicles ranging in size from 30 nm to several μm in diameter that are released from cells to facilitate intercellular communication (Thery et al., 2018). In addition to transferring trophic materials, EVs can facilitate the spread of pathogenic materials that can contribute to the spread of viruses, including HIV, hepatitis viruses C, coronavirus (CoV), and human adenovirus (HAdv) (Giannessi et al., 2020; Ipinmoroti and Matthews, 2020), as well as aggregation-prone proteins involved in neurodegenerative diseases including Aβ, tau, and α-synuclein (Saman et al., 2012; Emmanouilidou et al., 2010). EVs can also transfer pathogenic microRNAs (miRNAs). For example, EV- associated miR-139-5p has been shown to contribute to the pathophysiology of MDD, and EVs from individuals with MDD can induce behavioral abnormalities relevant to depression via miR-139-5p-regulated neurogenesis when injected into mice (Wei et al., 2020).

EVs are enriched with ceramide as compared with the cellular membranes from which they are derived (Trajkovic et al., 2008). The generation of ceramide on one side of a lipid membrane bilayer creates a mismatch in surface tension that coupled with the small size of the ceramide polar head group forms spontaneous negative curvatures (Lopez-Montero et al., 2007). These properties, and thus the enzyme neutral sphingomyelinase 2 (nSMase2) that hydrolyzes sphingomyelin to ceramide, are critical for the biogenesis of extracellular vesicles (Trajkovic et al., 2008). Aberrant activation of nSMase2 has been implicated in multiple neurological disorders, including age-related neurodegeneration, Alzheimer's disease, HIV-associated dementia, atherosclerosis, and ischemia-reperfusion injury (Haughey et al., 2004; Williams et al., 2021). Specifically relevant to this study, enhanced sphingomyelinase activity and increased ceramide levels have been described in both HIV and MDD patients (Haughey et al., 2004; Haughey et al., 2008; Dinoff et al., 2017; Muhle et al., 2019).

The present study was designed to determine if EcoHIV-infected mice exhibit behavioral abnormalities relevant to depression, in addition to the previously reported cognitive deficits resembling those in virally suppressed PLH (Gu et al., 2018; Nedelcovych et al., 2017; Kelschenbach et al., 2019; Kim et al., 2019), and if inhibition of nSMase2 with (*R*)-(1-(3-(3,4-dimethoxyphenyl)-2,6-dimethylimidazo[1,2-*b*]pyridazin-8-yl) pyrrolidin-3-yl)-carbamate (PDDC), our newly discovered oral and brain penetrable nSMase2 inhibitor (Rojas et al., 2019), could reverse CI and behavioral abnormalities in this model. Effects of EcoHIV infection and nSMase2 inhibition on behavioral phenotypes, brain enzymatic activity, sphingolipid levels, along with a comprehensive profiling of miRNAs cargo in brain-derived EVs are reported.

## 2. Results

### PDDC reversed memory deficit in EcoHIV infected mice.

Mice inoculated with EcoHIV by peritoneal injection develop cognitive impairment as determined by radial arm water maze (RAWM) and fear conditioning (FC) tests 3–4 weeks after infection (Kim et al., 2019). To determine if nSMase2 inhibition affects this impairment, mice were treated daily with 30 mg/kg PDDC starting at 28 days after infection for 12 days prior to RAWM testing. The training trials (T) measure the learning acuity of mice in finding the submerged platform and the 30 min retention trial (R) is a direct indicator of working memory (Gu et al., 2018). While EcoHIV-infected mice made significantly more errors in finding the submerged platform than uninfected mice, the performance of PDDC-treated EcoHIV-infected mice was statistically indistinguishable from that of uninfected mice and improved versus EcoHIV+Vehicle (Fig. 1A, 2-way ANOVA treatment effect $P < 0.01$). PDDC treatment alone did not affect the performance of mice in this test.

### PDDC was well-tolerated in EcoHIV-infected mice.

While PDDC was previously reported to be well-tolerated in normal mice (Sala et al., 2020), we monitored body weight and signs of distress such as hunched posture, lethargy, anorexia, dehydration, and rough hair coat in EcoHIV-infected mice chronically treated with PDDC. Neither EcoHIV infection nor PDDC treatment resulted in body weight changes or overt signs of toxicity (Fig. 1B).

### EcoHIV-infected mice displayed social avoidance and despair behavior which was reversed with PDDC.

While EcoHIV effects on cognition in infected mice have been relatively well established (Gu et al., 2018; Nedelcovych et al., 2017; Nedelcovych et al., 2019), we found that EcoHIV-infected mice also displayed behavioral abnormalities relevant to depression, and tested whether PDDC treatment affected these HIV-related psychiatric dysfunctions as well. The social interaction test (SIT) evaluates the natural curiosity of mice to interact with other mice. In the test, control mice treated either with vehicle or PDDC spent significantly more time in the chamber with the stranger mouse versus an inanimate toy. In contrast, EcoHIV-infected mice showed no preference for exploring the mouse or the toy (Fig. 1C). This social avoidance behavior was reversed to control levels with PDDC treatment. The forced swimming test (FST) evaluates despair behavior by testing the amount of time spent swimming and immobile in an inescapable tank, with immobility reflecting hopelessness or despair behavior. In the FST, the EcoHIV-infected mice exhibited increased immobility time versus the control mice, which was significantly reversed with PDDC treatment (Fig. 1D). To control for potential changes in locomotion and anxiety behavior in the mice, an open field test (OFT) was also performed. No differences were observed among the groups (Fig. 1, E and F). To confirm these results, a rotarod test was performed in a separate cohort of control mice treated with Vehicle or PDDC. No differences were observed between groups (Fig. S1).

### PDDC did not impact viral load in EcoHIV-infected mice.

EcoHIV-infected mice had detectable splenic viral load as measured by gag DNA levels at 45 days post-infection, and the viral burden was unaltered due to PDDC treatment (Fig. 1G).

### EcoHIV-infected mice exhibited increased brain nSMase2 activity which was normalized by PDDC.

Following completion of the behavior tests, mice were sacrificed and brain nSMase2 enzymatic activity was measured to examine the effect of EcoHIV infection on activity and to confirm PDDC target engagement. As compared to vehicle-treated Control mice, Control mice treated with PDDC exhibited significantly reduced nSMase2 activity levels, while EcoHIV-infected mice displayed significantly elevated nSMase2 activity levels. The EcoHIV-mediated increase in enzymatic activity was significantly reduced by PDDC treatment to levels below those observed in vehicle-treated Control and EcoHIV mice (Fig. 2).

### PDDC reduced ceramide and increased sphingomyelin concentrations in the cortex of EcoHIV-infected mice.

There were general trends of increased ceramide and decreased sphingomyelin (SM) concentrations in the cortex of EcoHIV-infected mice administered PDDC (Fig. 3A), that are consistent with the biological effects of inhibiting nSMase2. PDDC significantly reduced cortical concentrations of ceramide C16:0, C22:0, C24:0, dihydroceramide C18:0 and lactosyl ceramide C18:0 (Fig. 3B), and increased concentrations of SM C16:0, C16:1, C18:1, dihydro SM C16:0 and C22:0 (Fig. 3C).

### EcoHIV-infected mice exhibited elevated number of brain-derived EVs and altered miRNA content that were normalized by PDDC.

Transmission electron microscopy images revealed expected EV size and morphology in brain-derived EVs (bdEVs) (Fig. 4A). The number of bdEVs was elevated in EcoHIV-infected mice compared to control mice and normalized with PDDC treatment (Fig. 4B). Consistent with bdEV particle changes, EV-associated markers CD81 and CD9 were elevated in EcoHIV-infected mice and lowered by PDDC treatment (Fig. 4B). The percentage of larger bdEVs was slightly elevated in EcoHIV+Vehicle compared to other groups (Fig. 4C). To further characterize the bdEVs, their proteomics content was analyzed to determine the gene ontology (GO) of contained proteins. EV-related terms were found within the top 10 GO terms based on adjusted *p*-value in both mouse (Fig. S2A) and human (Fig. S2B) datasets. Moreover, 60 the top 100 most commonly reported EV-related proteins in the Exocarta database were identified in bdEVs from Control and EcoHIV mice +/− PDDC (Table S1).

RNA sequencing analyses (Fig. 5A) and qPCR validation (Fig. 5B) in the bdEVs showed that EcoHIV infection elevated the levels of 3 distinct miRNAs known to be altered in depression (Zhou et al., 2018; Cheng et al., 2018; Xu et al., 2015), miR-183-5p, miR-200c-3p, and miR-429-3p, along with miR-200b-3p, in both the prefrontal cortex (PFC) and hippocampus (HPC). PDDC treatment reduced these elevated miRNAs at or near control levels in the HPC and incompletely reduced levels in the PFC. qPCR analyses

normalized to internal references showed no changes to the HPC results but a diminishment of the PDDC-mediated changes in the PFC of EcoHIV mice (Fig. S3).

## 3. Discussion

EcoHIV/NDK was constructed by modifying the virus envelope region of HIV/NDK from HIV gp120 to the ecotropic mouse leukemia virus gp80 gene, thus switching viral tropism from humans to mice (Potash et al., 2005). Despite EcoHIV entering cells via a different receptor than HIV (Gu et al., 2018), there are strong behavioral and pathological similarities between mice chronically infected with EcoHIV and PLH, including the presence of latent-inducible virus in CD4^{+} T cells and expressed virus in microglia and peripheral macrophages, functional immune system responses, and the development of several HIV-associated chronic ailments including the gut, lung, vascular, and neurocognitive dysfunction resembling HIV-associated neurocognitive disorder (HAND) that are refractory to antiretroviral therapy (ART) (Table 1) (Gu et al., 2018; Nedelcovych et al., 2019; Potash et al., 2005; Hadas et al., 2007; Saylor et al., 2016; Kelschenbach et al., 2012; He et al., 2014). Uninvestigated to date, however, are alterations in behavioral dimensions relevant to depression in EcoHIV-infected mice, a critical feature to study given the very high prevalence of MDD in PLH. The present study is the first to show that EcoHIV-infected mice experience social avoidance and behavioral despair. These behavioral abnormalities in both the positive and negative valence system domains of the Research Domain Criteria (RDoC) framework are in line with domain disruptions observed in PLH (Andersen et al., 2020; Nanni et al., 2015). The present study shows that these behaviors are related to sphingolipid metabolism, as manipulation of nSMase2 activity and EV levels via PDDC treatment normalized EcoHIV-induced abnormalities independent of any changes in physical activity levels.

Sphingolipid metabolism is a highly dynamic process that regulates the formation of a number of bioactive lipid metabolites, including ceramides, ceramide-1-phosphate, sphingosine, sphingosine-1-phosphate (S1P) and glycosphingolipids (Pyne and Pyne, 2000). Sphingolipids, in particular ceramide, preferentially interact with cholesterol in plasma membranes forming highly ordered membrane microdomains that serve as platforms for cellular processes and second messenger systems (Brown and London, 2000). These membrane microdomains are themselves dynamic structures that can be rapidly modified in size and shape by the actions of nSMase2 to create ceramide (Xu et al., 2011). Ceramides are important for cell survival and essential for injury-induced cytokine production, but at high levels ceramides inhibit cell division and induce cellular dysfunction and apoptosis (Irie and Hirabayashi, 1998). Ceramides also activate protein phosphatases and kinases, enzymes involved in stress signaling cascades (Hannun, 1996). Over time, ceramide accumulation sensitizes neurons to oxidative damage, leading to neurodegeneration (Denisova et al., 1999). Indeed, increased ceramide concentrations have been reported in numerous neurological disorders including the neurological complications associated with HIV infection (Haughey et al., 2004; Haughey et al., 2008; Dinoff et al., 2017; Muhle et al., 2019; Tallon et al., 2021; Mielke et al., 2010).

Brain and CSF ceramide levels are elevated in PLH (Haughey et al., 2008). In vitro studies show that the HIV-1-mediated ceramide upregulation is due to the coat protein gp120 and the regulatory protein Tat, which enhance nSMase2 activity and subsequent ceramide production, leading to neuronal apoptosis (Haughey et al., 2004). The role of Tat was confirmed in a transgenic HIV-1 Tat mouse model that showed chronic low-level Tat production to be capable of inducing cortical ceramide accumulation and synaptic damage (Dickens et al., 2017). EcoHIV lacks the gp120-encoding portion of the HIV-1 *env* gene but it expresses functional Tat as indicated by efficient virus expression in mice and production of anti-Tat antibodies by infected mice (Gu et al., 2018; Potash et al., 2005). Thus, the trend elevations in ceramides in EcoHIV-infected mice are likely due, at least in part, to Tat expression by the virus. HIV Nef protein, which interacts with membrane lipid rafts (Mukhamedova et al., 2019) and is expressed by EcoHIV (Kelschenbach et al., 2019), could also be involved.

While the monoamine depletion hypothesis remains the leading explanation for the biochemical basis of MDD, the disease is far more complex than dysregulation of one neurotransmitter family. In fact, a host of preclinical and clinical studies implicate ceramide as a contributing factor to MDD (Dinoff et al., 2017; Brunkhorst-Kanaan et al., 2019). MDD is characterized by a reduction in hippocampal volume (Videbech and Ravnkilde, 2004), due to increased hippocampal cell death and/or decreased hippocampal neurogenesis. Interestingly, hippocampal neurogenesis-deficient mice exhibit behavioral abnormalities relevant to depression (Snyder et al., 2011), application of ceramides to hippocampal neurons prevents neurogenesis (Gulbins et al., 2016), and direct injection of ceramide into the hippocampus results in anhedonia-like and anxiety-like behaviors in mice (Gulbins et al., 2013). Relevant to these findings, EcoHIV infection was shown to reduce mouse neurogenesis both in neuronal progenitor cell (NPC) culture models and two weeks after infection of mice (Skowronska et al., 2018). This process too could be mediated by EcoHIV-expressed Tat (Fan et al., 2016) and, as shown here, may involve overexpression of ceramides.

In addition to regulating proliferative and apoptotic cellular processes, ceramides are critical mediators of EV biogenesis. Owing to a high degree of saturation, ceramides pack tightly together forming highly structured membrane microdomains that are asymmetrically distributed to one side of the plasma membrane. The small size of the ceramide polar head group and the asymmetric distribution of ceramides caused membrane curvature through the formation of inverted hexagonal phases (Lopez-Montero et al., 2007) that facilitates the formation of intraluminal vesicles, which are released from cells as EVs. EVs contain a variety of cargo, which can be beneficial or detrimental to cell survival. Taking into account the increased ceramide levels observed in individuals with MDD (Dinoff et al., 2017) or HIV with CI (Haughey et al., 2004; Bandaru et al., 2007), it is unsurprising that increased levels of brain-derived EVs isolated from plasma have also been observed in both conditions (Wallensten et al., 2021; Pulliam et al., 2019).

Here we show that similar to individuals with HIV or MDD (Wallensten et al., 2021; Guha et al., 2019), EcoHIV-infected mice experience increased bdEV levels compared to normal controls and that nSMase2 inhibition with PDDC completely normalizes this abnormality.

Inhibition of EV release via nSMase2 inhibition has shown positive preclinical data in many indications, including cancer and neurodegenerative, inflammatory, and infectious diseases (Tallon et al., 2021), but this is the first study to explore the therapeutic potential of nSMase2 inhibition in a preclinical model of HIV-associated depression and cognitive impairment. bdEVs from EcoHIV+Vehicle mice showed fewer EVs ranging from 50 to 70 nm and more from 80 to 100 nm compared to other groups. This finding is not likely due to contamination of our EV sample with virus particles, as the average HIV particle size is usually above 100 nm (Giannessi et al., 2020) and EcoHIV particles are larger that HIV particles (Potash et al., 2005). To our knowledge, no studies have explored the importance of bdEV size shift in infectious diseases, and future studies will explore the implications of this observation. In addition to transmission electron microscopy, flow cytometry, and single particle interferometric reflectance imaging, proteomics analyses confirmed the presence of EVs in brain samples. The top 10 GO classification terms from the mouse and human STRING databases revealed enrichment for EV-related terms (Crescitelli et al., 2020), including cellular entity and vesicle, in both species. We hypothesize that more of the hits from the human GO terms are directly associated with EVs (i.e. vesicle, extracellular vesicle, extracellular exosome) because the human data sets are more highly utilized and honed on the STRING database. It is important to note that in all of these characterizations, samples were pooled from 6 to 8 mice in order to collect enough material to run all analyses. Although it is reassuring to achieve confirmatory results through multiple methodologies, future large-scale studies are required to confirm these findings.

Although PDDC treatment caused a significant reduction in nSMase2 activity levels below those observed in vehicle-treated Controls, the nSMase2 inhibitor did not alter neurobehavioral phenotypes in Control mice. This was unsurprising in the tests related to depressive-like behaviors, as there was no deficit to correct, but previous studies have also reported a motor coordination deficit (Tan et al., 2018) and cognitive impairment (Tabatadze et al., 2010) in normal mice due to nSMase2 inhibition with GW4869. The study reporting GW4869-mediated motor coordination deficits utilized an intrastriatal injection of GW4869, but the dose was unspecified (Tan et al., 2018). Direct brain injection of high drug doses could mediate off-target toxic and/or sedating effects unrelated to nSMase2 inhibition. Using both open field and rotarod tests, we thoroughly demonstrate that PDDC treatment did not impact motor function, validating the utility of our tasks that measure depression-like behaviors that assume equal motor abilities between groups. The previously published study claiming a GW4869-mediated cognitive impairment showed a very modest effect, as a deficit related to the formation of spatial reference memory was observed in only a very specific subset of trials, and no deficits were observed in tasks measuring episodic memory and spatial recognition memory (Tabatadze et al., 2010). Here we show no impact of nSMase2 inhibition on spatial learning and memory in control mice. It is critical to note that differences between our study and previous studies could be due to the utility of different nSMase2 inhibitors. GW4869 and PDDC have different nSMase2 binding sites, the juxtamembrane region linking the C-terminal domain and the N-terminal domain (Airola et al., 2017) and the phosphatidyl serine regulatory site on the N-terminal domain (Sala et al., 2020), respectively, which could generate dissimilar side effects. PDDC treatment also led to changes in one ceramide species (LacCer d18:1/18:0) and one sphingomyelin

species (SM d18.1:16.1), but given that neither of these species were altered between Control+Vehicle and EcoHIV+Vehicle groups, it is unlikely that they contribute to the positive neurobehavioral effects observed in the present study.

Given the nefarious role that EVs can play in disease pathogenesis (Tallon et al., 2021), there is a growing interest in examining the contents of EVs in many disorders, including depression, HIV, and HAND (Pulliam et al., 2019; Saeedi et al., 2019). EVs are carriers of miRNA, and the nervous system expresses approximately 70% of all miRNA (Nowak and Michlewski, 2013). miRNAs typically regulate gene expression via enhancing or suppressing mRNA translation, and these small non-coding RNAs, which are thought to be shuttled between cells via EVs (Valadi et al., 2007), have been implicated in multiple diseases including depression and cognitive decline. To our knowledge, however, this is the first study to examine bdEV miRNA content in a preclinical model of HIV-associated CI and depression. We report four miRNAs, including miR-429-3p, miR-200c-3p, miR-183-5p, and miR-200b-3p, that are upregulated in bdEVs of EcoHIV-infected mice and normalized by PDDC treatment.

In line with our findings, it was previously shown that rats not exhibiting learned helplessness following shock stressors, in turn indicating resistance to depression, had significant and > 75% reductions in frontal cortex miR-429, miR-200c, and miR-183 content (Dwivedi et al., 2015). Similarly, amygdalae levels of miR-183 were elevated in mice subjected to acute immobilization stress (Meerson et al., 2010). A member of the miR-183 family, miR-183-5p, targets TET1, the loss of which confers resistance to stress-induced behavior abnormalities including passive behavioral despair as measured by the forced swim and tail suspension tests in mice (Cheng et al., 2018). An additional target of miR-183 is PFN2, which is significantly upregulated in humans with MDD (Martins-de-Souza et al., 2012) and encodes an actin-binding protein that regulates dendritic spine morphology (Michaelsen et al., 2010). The miRNA 200 family consists of 5 members, among them, miR-429 and miR-200c, both of which were significantly altered in EcoHIV-infected mice. Targets of both miR-429-3p and miR-200c-3p are ZEB1 and ETF1, which have been implicated in MDD (Xu et al., 2015) and bipolar II disorder (Kao et al., 2016), respectively. Another target of both miR-429 and miR-200c is DDX3X, a translational regulator critical to neurogenesis that is frequently mutated in individuals with intellectual disabilities (Lennox et al., 2020). miR-200c-3p also regulates inflammation, a critical pathological mediator of both depression and HIV (Rivera-Rivera et al., 2016). Epileptic rats experienced elevations in hippocampal miR-200c-3p and the inflammatory cytokines TNF-$\alpha$, IL-1$\beta$, and IL-6, which were reversed via inhibition of the miRNA (Du et al., 2019).

It is important to note that several studies have reported miRNA results that are in opposition to our results and those highlighted above. Following stress-induced behavioral abnormalities relevant to depression, mice were reported to have reduced miR-200c-3p and miR-429-3p levels in the ventral tegmental area (Sun et al., 2018) and reduced levels of miR-429 in the prefrontal cortex (Satyanarayanan et al., 2019). We did not observe changes in miR-139-5p, which was recently shown to be elevated in MDD patients and in a mouse model of the disease induced by injection of exosomes from patients with MDD (Wei et al., 2020). It is likely that different methodologies, brain regions examined, and our analysis

of EV-derived miRNA versus miRNA in brain homogenates account for these differences. Finally, a study of MDD patients showed that miR-183 levels were elevated following 12 weeks of antidepressant treatment (Bocchio-Chiavetto et al., 2013), but the success of the treatment and alleviation of depressive symptoms were not recorded.

Recent advances in HIV treatment have made prolonged viral suppression possible for patients with continued access to stable ART. Unfortunately, however, MDD prevalence is still high in PLH who are on ART (Algoodkar et al., 2017), and comorbid depression in PLH decreases ART compliance rates by over 40% (Uthman et al., 2014). Given the elevated rates of CI and somatic aging-related diseases, including cancer, diabetes, and heart disease, in individuals with MDD (Verhoeven et al., 2014), along with the nearly 2-fold higher incidence of MDD in HIV-positive versus the general population (Ciesla and Roberts, 2001), examination of mood-related changes and the development of novel therapies is critical for this patient population.

CI and depression are comorbidities that commonly manifest in PLH, and here we confirm that EcoHIV-infected mice experience similarly broad behavioral phenotypes. The present findings in the EcoHIV-infected mice model suggest that similar to HAND, depressive symptoms may also be exacerbated by HIV infection due to ceramide dysregulation. The ceramide imbalance and elevated bdEV release observed in EcoHIV-infected mice in the present study closely mimic results observed in PLH, patients of depression, and individuals with CI, and strongly supports the development of a nSMase2 inhibitor for the treatment of comorbid depression and CI in PLH.

## 4. Methods

### Mice.

Male 8–12-week-old C57BL/6 J mice (Jackson Laboratory) were purchased from Jackson Laboratories. Rooms were maintained at 21 °C under a 12-h light-dark cycle with ad libitum access to water and rodent chow, and body weight was monitored weekly.

### EcoHIV propagation and infection of mice.

EcoHIV was propagated and mice were infected via intraperitoneal injection of virus stock as previously described (Nedelcovych et al., 2019; Potash et al., 2005). Briefly, HEK293T cells were transfected with plasmid DNA containing a previously described construct of EcoHIV/NDK harboring the V5C5 fragment of gp120 (Gu et al., 2018; Kim et al., 2019; Potash et al., 2005). EcoHIV was then isolated from culture media by centrifugation and concentrations measured by p24 ELISA (Advanced Biosciences Laboratory, Rockville, MD). For all experimental endpoints, mice were inoculated with EcoHIV ($2–4 \times 10^6$ pg p24, i.p.) or a sham injection of saline.

### Drug treatment.

Beginning at 3–4 weeks post-EcoHIV infection and until the time of sacrifice, mice were dosed either orally via gavage (RAWM) or intraperitoneally (all other experiments), both previously published and efficacious delivery methods (Rojas et al., 2019; Sala et al., 2020),

with either vehicle or the small molecule nSMase2 inhibitor PDDC. PDDC was formulated in either *N*-methyl-2-pyrrolidone (NMP) or dimethyl sulfoxide (DMSO)–Tween 80–saline (2.5:5:92.5 *v*/v/v) and delivered at a dose of 30 mg/kg. The dose of 30 mg/kg PDDC was chosen because it achieves brain levels >2-fold higher than its $IC_{50}$ and results in significant inhibition of brain nSMase2 activity (Rojas et al., 2019). A lower 10 mg/kg dose was piloted but exhibited lower brain nSMase2 inhibition (24.8% at 10 mg/kg versus 43.8% at 30 mg/kg).

### Behavioral studies.

Behavioral studies were initiated following at least 10 days of daily drug treatment. The RAWM test was administered in a pool of opaque water containing 6 swimming lanes and a hidden platform as described (Petrone et al., 2003). Briefly, each testing group contained between 8 and 10 mice; RAWM testing consisted of 4 training trials (T) of 60s and 1 post-training 60s retention trial (R) administered after 30 min rest. The hidden platform was rotated randomly to a different arm each test day to ensure that mice used working memory to locate the platform. Testing was considered complete when control mice reached asymptotic performance of one error or fewer in finding the hidden platform on trials T4 and R. Errors for the last three days of testing were averaged and used for statistical analysis. The hidden platform tests were followed by measuring the time (latency) it took for treated and control mice to find a visible platform, as a control for possible effects of treatment on animal vision, motivation, or ability to swim to the platform.

The FST was performed in a clear glass cylinder filled with tap water at 25 °C following published procedures (Fitzgerald et al., 2019). The test lasted for 6 min long, divided into pretest (the first 2 min) and test (the last 4 min). Water was changed after every session to avoid any influence on the next mouse. The duration of immobility was coded during the last 4 min test by an investigator who was blinded to the study conditions. Time was recorded as "immobile" if the mouse was floating with the absence of any movement except for those necessary for keeping the nose above water.

The three-chamber social interaction test (SIT) was administered to evaluate social avoidance behaviors using published protocols with minor modifications (Zhu et al., 2019). Briefly, mice were placed in a three-chamber apparatus (40 cm width × 20 cm height × 26 cm depth) in which both side chambers contained a plastic cage in the corner. The trial consisted of three sessions. In the first session, test mouse was habituated for 10 min in the center chamber, and mouse was allowed to freely explore all three chambers including two side chambers in the second 10 min session. The test mouse was then gently confined in the center chamber while a same strain stranger mouse (stranger) was placed in one of the two plastic cages, and an inanimate object (inanimate) was placed into another cage in the other side chamber. In the third session, the test mouse was allowed to freely explore all three chambers for 10 min. Mouse behaviors were video-recorded and the trajectory of mouse ambulation was automatically determined by a video tracking system, TopScan 3.0 (CleverSys, Reston, VA, USA).

The OFT was performed to measure overall activity levels as described previously (Niwa et al., 2010). Briefly, mice were gently placed on the center of the open field apparatus

and allowed to freely move for 30 min. A Photobeam Activity System (PAS–Open Field, San Diego Instruments) was used to measure the locomotion activity of the mouse. The PAS system consisted of two vertically stacked frames, each containing infrared lasers arranged in a $16 \times 16$ grid, which detected mouse movement. The open field box and surrounding photobeam apparatus were housed in a ventilated cabinet. Single-beam breaks were automatically recorded as "counts" and the PAS system automatically started recording counts once the mouse started moving. The total counts and time in which mouse exploring the periphery and the center of the arena were recorded and used for analyses.

The rotarod test was performed in a separate cohort of control mice +/− PDDC to examine motor coordination following chronic nSMase2 administration. Briefly, following 12 days of vehicle or PDDC injections, mice underwent 3 consecutive days of rotarod testing wherein the animal was placed on a horizontal rod that rotates about its long axis at a speed starting at 4 and accelerating at regularly timed intervals. Each mouse underwent 3 trials/day with a rest of at least 2 min between trials. Latency to fall and speed at the time of fall were recorded and averaged over the 3 trials/day.

### nSMase2 activity.

Primary cortices from EcoHIV mice, treated with vehicle or PDDC, were dissected and analyzed for nSMase2 activity using a modification of published protocols (Rojas et al., 2018). Briefly, mice cortices were homogenized in ice-cold Tris-HCl buffer (0.1 M, pH 7.5) containing 250 mM sucrose, 10 mM EGTA (Research Products International, Prospect, IL), 100 μM sodium molybdate and protease inhibitors (Cell Signaling, Danvers, MA) using BioMasher II and then sonicated using Kontes' Micro Ultrasonic Cell Disrupter (three pulses of 15 s duration on ice with 30s between pulses). The resulting lysates were used for both nSMase2 activity measurements and protein analysis. nSMase2 activity measurements were initiated upon the addition of sphingomyelin (SM) and coupling enzymes in the Amplex Red system as previously detailed (Rojas et al., 2018). Total protein measurements were carried as per manufacturer's instructions using Bio-Rad's Detergent Compatible Protein Assay kit and data presented as relative fluorescent units (RFU)/mg/h (h).

### Viral burden measurements.

The procedures for harvesting spleen, preparing cellular DNA, and detecting EcoHIV/NDK *gag* DNA by real-time quantitative PCR (qPCR) were performed as previously described (Hadas et al., 2007; Kelschenbach et al., 2012). Splenic gag DNA was measured by isolating DNA from $5 \times 10^6$ cells and comparing copy number to the internal GAPDH reference. Custom Taqman QPCR primers were purchased from Applied Biosystems (ABI, Foster City, California, USA) and amplification was conducted in an Applied Biosystems 7500 instrument. EcoHIV/NDK DNA from the *gag* gene region was detected with forward primer 5′–TGGGACCACAGGCTACAC TAGA–3′, reverse primer 5′–CAGCCAAAACTCTTGCTTTATGG–3′ and probe 5′–TGATGACAGCATGCCAGGGAGTGG–3′. DNA content was standardized by amplification of murine β globin (forward primer, 5′–GGTTTCCTTCCCCTGGCTAT–3′; reverse primer, 5′–CGCTTCCCC TTTCCTTCTG–3′; probe, 5′–CTGCTCAACCTTCC– 3′). Samples for qPCR were run in duplicate in the AB7300 real time thermal cycler

(Thermo Fisher Scientific). DNA qPCR reactions were normalized by amplification of glyceraldehyde 3-phosphate dehydrogenase (GAPDH) using a kit from Applied Biosystems (ABI, Foster City, CA). Data analysis was performed with the 7300 System software according to the manufacturer's instructions.

### Lipid extractions.

Lipid extractions of tissue samples were performed using a modified Bligh & Dyer method (Bligh and Dyer, 1959). Briefly, tissue samples were weighed and homogenized in water (10×) followed by the addition of methanol (3×) containing internal standards ceramide (d18:1/12:0) and sphingomyelin (d18:1/12:0) (Avanti Polar Lipids, Alabaster, AL, USA) (Haughey et al., 2004) at a concentration of 1.3 μg/mL. Chloroform (4×) was then added to the mixture. After the clear phase separation, organic layers containing crude lipid extracts were collected and dried in a nitrogen evaporator (Organomation, Berlin, MA, USA) and stored at −80 °C. Dried extracts were resuspended in pure methanol prior to analysis.

### Ceramide and sphingomyelin LC-ESI-MS/MS analysis.

Ceramide and sphingomyelin were separated on a C18 reverse-phase column (2.6 μm, 50 × 2.1 mm) with an ULTRA HPLC In-Line Filter (0.5 μm Depth Filter × 0.004 in ID) (Phenomenex, Torrance, CA, USA) using a Shimadzu ultra-fast liquid chromatography (UFLC) system (Shimadzu, Nakagyo-ku, Kyoto, Japan). UFLC was coupled to a hybrid triple quadrupole LIT (linear ion trap) mass spectrometer 4000 QTRAP system equipped with Turbo Ion Spray (SCIEX, Foster City, CA, USA). Positive electrospray Ionization (ESI, +ve) was used to ionize these lipid species and individual ceramide and sphingomyelin species were detected by multiple reaction monitoring (MRM). Instrument conditions and HPLC parameters were similar to those described in previous studies (Bandaru et al., 2007). In order to monitor the instrument condition over the run of samples, quality control (QC) samples were injected in every 10 injections. Eight-point calibration curves (0.1–1000 ng/mL) were constructed by plotting area under the curve (AUC) for each ceramide calibration standard d18:1/C16:0, d18:1/C18:0, d18:1/C20:0, d18:1/C22:0, d18:1/C24:0, and SM calibrations standards C16:0, C18:0, C20:0, C22:0 and C24:0 (Avanti polar lipids, Alabaster, AL, USA). Correlation coefficients for standard curves were > 0.999. Ceramide and sphingomyelin concentrations were calculated by fitting the identified individual species to these standard curves based on acyl chain length. Instrument control and data acquisition were performed by using Analyst (version 1.4.2, SCIEX Inc. Thornhill, Ontario, Canada) and data analysis were completed using MultiQuant software (version 2.0, SCIEX, Thornhill, ON, Canada).

### EV separation from brain tissue.

EVs were isolated from PFC and HPC tissues as previously described (Huang et al., 2020). Briefly, mice were perfused with ice cold PBS and brains were snap frozen until EV separation. To isolate EVs, frozen tissue was weighed and briefly sliced on dry ice and then incubated in 75 U/mL collagenase type 3 (Worthington #CLS-3, S8P18814) in Hibernate-E solution for 15 min at 37 °C. Phos-STOP and Complete Protease Inhibitor (SigmaAldrich PS/PI 4906837001/11697498001) solution were added to stop digestion. The dissociated tissue was spun at 300 ×$g$ for 10 min at 4 °C. Supernatant was transferred to

a fresh tube and spun at 2000 ×g for 15 min at 4 °C to remove apoptotic bodies. Cell-free supernatant was filtered through a 0.22 μm filter (Millipore Sigma, SLGS033SS) gently and slowly for further depletion of large cell debris and spun at 10,000 ×g for 30 min at 4 °C (Thermo Fisher swinging-bucket rotor model TH-641, k-factor 114, acceleration and deceleration settings of 9, using Ultra-Clear tubes with 5 mL capacity) to pellet large EVs. The 10,000 × g supernatant was concentrated by 100 kilodalton (kDa) MWCO protein concentrator (Thermo Fisher 88,524) from 12 mL to 0.5 mL and loaded onto a size-exclusion chromatography column (qEV original, IZON Science SP1-USD, Christchurch, New Zealand) and eluted by PBS. 0.5 mL fractions were collected. A total of 2 mL eluate (Fractions 7–10) were pooled and ultracentrifuged for 70 min at 110,000 × g (average) at 4 °C (swinging-bucket rotor model TH-641, Thermo Fisher, k factor 114 at max speed, acceleration and deceleration settings of 9, using thinwall poly-propylene tubes with 13.2 mL capacity). Supernatant was removed, and the pellet was resuspended in 150 μL PBS as the purified EV fraction. Fractions were stored at −80 °C.

### Transmission electron microscopy.

EV preparations (10 μL) were adsorbed to glow-discharged 400 mesh ultra-thin carbon-coated grids (EMS CF400-CU-UL) for 2 min, followed by 3 quick rinses in TBS and staining in 1% uranyl acetate with 0.05 Tylose. After being aspirated and dried, Grids were imaged on a Hitachi 7600 TEM operating at 80 kV with an AMT XR80 CCD (8 megapixels).

### Nano flow FCM analysis.

The concentration of EV were detected on high sensitivity flow cytometry (HSFCM) as per manufacturer's instructions and as previously described (Arab et al., 2021). The photon counting avalanche photodiodes (APDs) were used for detection of the side scatter (SSC) of individual EVs. The concentration of each EV sample was determined by employing 200 nm PE and AF488 fluorophore conjugated phosphatidylserine beads (NanoFCM Inc) of known particle concentration to calibrate the sample flow rate. Each sample were diluted and collected for 1 min to record all the particles passing by the detector.

### Single particle interferometric reflectance imaging (SP-IRIS).

Measurements were performed per manufacturer's instructions and as previously described (Arab et al., 2021). Briefly, A total of 15 μL EVs were diluted in 22.5 μL incubation buffer (IB). Diluted EVs were then incubated over-night at room temperature on ExoView chips (NanoView Biosciences, Cat # EV-TETRA-M2) printed with anti-mouse CD81, anti-mouse CD9, and isotype controls. After incubation, chips were washed with IB 4 times for 3 min each under gentle horizontal agitation at 500 rpm. Chips were then immersed twice in rinse buffer for approximately 5 s each and removed at a 45-degree angle to allow the liquid to vacate the chip. All reagents were supplied by NanoView Biosciences (Brighton,MA, Cat # EV-TETRA-M2). Chips were imaged in the ExoView scanner (NanoView Biosciences, Brighton, MA) by interferometric reflectance imaging detection. Data were analyzed using NanoViewer 2.8.10 Software (NanoView Biosciences).

### 4.1. Mass spectrometry analysis

**Sample preparation, protein digest, peptide TMT labeling.—**Protein from brain-derived extracellular vesicles (bdEVs) from the HPC were extracted using RIPA buffer (Cell Signaling Technology), disulfide bonds reduced using 50 mM dithiothreitol (Sigma, D0632) and cysteine residues alkylated with iodoacetamide (Sigma, I1149) as previously described (Arab et al., 2019). Resulting protein lysat were precipitated with Trichloroacetic acid (TCA) reagent (Sigma, T0699). Briefly, sample were supplemented with 10% of TCA in aceton solution in a ratio of (1:8, *V*/V). After precipitation, pellets were resuspended in 50 mM ammonium bicarbonate containing 10% acetonitrile, sonicated for 10 min, and pH was adjusted to 7.8–8.0 using Tris Hydrochloryde, pH 8.0. Trypsin (Pierce, 90,057) at a concentration of 12 ng/mL was used for digestion over night at 37 °C. The resulting peptides were further cleaned up using C18 ZipTips (Millipore, ZTC18S096). Briefly, ZipTip cones were washed with 50% acetonitrile (ACN) and equilibrated using 0.1% formic acid (FA) solution. The peptides were linked to the C18 phase tips by pipetting ups and downs 20 times, washed with 0.1% FA solution, eluted into a clean tube using ACN:FA 0.1% (80:20, V/V), and completly dried under vacuum. Isobaric labeling of the digested peptides was accomplished with 10-plex TMT reagents (Thermo Fisher Scientific). Reagents were reconstituted in 20 μL ACN and 1/2 was added to the digested peptides reconstituted in 12.5 μL of 60 mM triethylammonium bicarbonate beforehand. The mixture was incubated at room temperature (≈ 22 °C) for 1 h and the reaction was quenched by adding 2 μL of 5% hydroxylamine and incubated for an additional 15 min. All TMT-labeled peptides were combined into total ~ <8μg and dried to ~25uL. Samples were cleaned on Pierce Detergent removal columns and peptides were eluted in 300 μL of a solution composed of 8% Triethylammonium bicarbonate, 0.1% Trifluoroacetic acid and 92% water. Prior to mass spectrometer analysis, peptides were de-salted on u-HLB Oasis plates (Waters), eluted in a buffer containing 60% acetonitrile and 0.1%TFA and dried completely under a vaccum.

**Liquid chromatography separation and tandem mass spectrometry (LC-MS/MS).—**Desalted peptides were reconstituted in 40 μL solution buffer containing 2% ACN and 0.1% FA, then loaded on MS/MS plate. Peptides were separated using nano-LC-Orbitrap-Lumos-ETD in FTFT (Thermo Fisher Scientific) interfaced with a reverse chromatography phase EasyLC1200 series equipped with ProntoSIL-120–5-C18 H BISCHOFF column (75 μm × 150 mm, 3 μm). To separate the digested peptides, an increase concentration of ACN in 0.1% FA from 2%–90% for over 78 min at a flow rate of 300 nl/min was utilized. A voltage of 2.4 kV was applied by the liquid junction in order to electrospray the eluent into an Orbitrap-Lumos-Fusion mass spectrometer through a 1 μm emitter tip. For MS acquisition, in data dependent mode was defined to analyze the 15 most intense ions (Top 15) with dynamic exclusion of 15 s. Analyses were performed at resolution power of 120,000 FWHM. For full scan MS, the scan range was between 375 and 1600 Da *m/z.* For tandem mass spectrometry (MS/MS), precursor ions were individually isolated with 0.7 Da, fragmented (MS/MS) using a Higher-energy C-trap Dissociation (HCD) with activation collision energy set at 38. Fragment ions were analyzed at a resolution of 60,000 FWHM.

**Raw data processing and analysis.**—All the tandem MS/MS spectra (signal/noise >2) were processed by Proteome Discoverer (v2.4 ThermoFisher Scientific) using Files RC option (recalibration with appropriate database). MS/MS spectra were searched with Mascot v.2.6.2 (Matrix Science, London, UK) and proteins were identified by searching against 2021_204_ *Mus musculus* and HIV_NCBI_210512 databases with 1% false discovery rate (FDR) for peptide identifications. Trypsin specificity was used for the digestion, with up to two missed cleavages. Methionine oxidation and deamidation ON no were selected as the variable modifications. Carbamidomethylation of cysteines and TMT-label modifications of N-termini and lysine were set as fixed modification. Based on a concatenated decoy database search, Proteome Discoverer-Percolator was used for validation of identified peptides with a confidence threshold of 1% FDR and for the protein and peptide ratio calculation. Furthermore, only unique and Rank 1 peptide were considered for calculation and only unmodified peptides were used for normalization and ratio calculation. For quantification Proteome Discoverer used TMT reporter ions from peptide matched spectrum (PSM), and PSMs with reporter signal/noise >5 and an isolation interference <25 were used. Protein quantification was based on the normalized median ratio of all spectra of tagged peptides from the same protein (Herbrich et al., 2013). Peptides modified with methionine oxidation, asparagine and glutamine deamidation were excluded from normalization and ratios calculations, but considered for Protein Roll-Up (all peptides used for roll-up). STRING functional protein association networks version 11.5 was used to determine the most enriched cellular component associated with the identified protein in hippocampus region. Searches were conducted twice, by selecting *M. musculus* as organism and then *Homo sapiens* as organism. GO terms were ranked by adjusted *p*-value.

**RNA isolation and quality control.**—RNA was purified by miRNeasy Mini Kit solutions (Qiagen 217,004) and Zymo-Spin I Columns (Zymo Research C1003–50) according to the manufacturer's instructions. The small RNA profiles of samples were analyzed using capillary electrophoresis by RNA 6000 Pico Kit (Agilent Technologies 5067–1513) on a Fragment Analyzer (Advanced Analytical).

**Small RNA sequencing.**—Given the relatively low yield of bdEVs in the PFC and HPC, samples were pooled from 6 to 8 mice. Small RNA libraries were constructed from 8 μL of RNA extracted from bdEVs using the CATS Small RNA-seq Kit (Diagenode C05010040). Indexes were attached using the D-Plex 24 Single Indexes for Illumina (Diagenode C05030010) according to the manufacturer's protocol and as previously published. The yield and size distribution of the small RNA libraries were assessed using the Fragment Analyzer instrument with DNA 1000 chip (Agilent Technologies 5067–1504). After the library size selection by BluePippin (Sage Science) from 160 bp–190 bp, multiplexed libraries were equally pooled to 2 nM based on their fragment analyzer concentrations. The concentration of the pooled library was further verified via qPCR using KAPA Library Quantification Kits (Roche KK4824). The libraries were then used for deep sequencing on NextSeq 500 system (Illumina SY-415-1002) using the NextSeq 500/550 High Output Kit v2.5 kit (75 Cycles) (Illumina 20,024,906).

**RNA sequencing data analysis.—**Original BAM files were converted into FASTQ format using picard tools (SamToFastq command). Reads shorter than 15 nt were removed from the raw FASTQ data using cutadapt software v1.18. The size-selected reads were aligned to mouse reference transcriptomes using Bowtie software (1 mismatch tolerance) in a sequential manner. Specifically, reads were first mapped to rRNA, tRNA, RN7S, snRNA, snoRNA, scaRNA, VT-RNA, Y-RNA as well as the mitochondrial genome. All reads which did not map to the above RNA species were aligned to mouse miRNA references (miRBase 22 release). The remaining reads were further aligned to protein-coding mRNAs and long non-coding RNA (lncRNA) references (GENCODE Release 29). The numbers of reads mapped to each RNA type were extracted using eXpress software based on a previous publication (Roberts and Pachter, 2013). Protein-coding and long-coding RNA results were not interpreted given that utilization of library inserts <50 bp would yield incomplete results. Differential gene expression was quantified using R/Bioconductor packages DESeq or DESeq2 as described (Love et al., 2014). RefFinder was used for evaluating and screening internal reference genes from small RNA sequencing datasets.

**Individual RT-qPCR assays.—**Individual TaqMan miRNA qPCR assays were performed as previously described (Witwer et al., 2011) on bdEV samples from HPC and PFC using Thermo Fisher primers: miR-183-5p (Assay ID # 002269), miR-200c-3p (# 002300), miR-429-3p (# 001077), miR-200b-3p (# 002251). Data were adjusted to the geometric mean of Cq values of selected internal reference genes: miR-99b-5p (Assay ID # 000436), miR-485–5p (# 000436), and miR-125a-5p (# 002198).

**Data availability and EV-TRACK.—**Nucleic acid sequencing data have been deposited with the Gene Expression Omnibus, accession GSE182743. We have submitted all relevant data of our experiments to the EV-TRACK knowledgebase (EV-TRACK ID: EV210241) (Consortium et al., 2017).

**Statistics.—**Statistical analyses were completed using GraphPad Prism 6.0. As indicated for each experiment, differences among more than two groups were determined using two-way analysis of variance (ANOVA), followed by the Tukey multiple comparison test. The Student's *t*-test was used in comparing two sets of data. A value of $P < 0.05$ was considered significant.

**Study Approval.—**All protocols were approved by the Johns Hopkins Institutional Animal Care and Use Committee or the Icahn School of Medicine Institutional Animal Care and Use Committee, and in full compliance with NIH guidelines.

## Supplementary Material

Refer to Web version on PubMed Central for supplementary material.

## Acknowledgments

## References

Airola MV, Shanbhogue P, Shamseddine AA, Guja KE, Senkal CE, Maini R, et al. , 2017. Structure of human nSMase2 reveals an interdomain allosteric activation mechanism for ceramide generation. Proc. Natl. Acad. Sci. U. S. A 114 (28), E5549–E5558. [PubMed: 28652336]

Algoodkar S, Kidangazhiathmana A, Rejani PP, Shaji KS, 2017. Prevalence and factors associated with depression among clinically stable people living with HIV/AIDS on antiretroviral therapy. Indian J. Psychol. Med 39 (6), 789–793. [PubMed: 29284813]

Anagnostopoulos A, Ledergerber B, Jaccard R, Shaw SA, Stoeckle M, Bernasconi E, et al. , 2015. Frequency of and risk factors for depression among participants in the Swiss HIV cohort study (SHCS). PLoS One 10 (10), e0140943. [PubMed: 26492488]

Andersen LS, Joska JA, Magidson JF, O'Cleirigh C, Lee JS, Kagee A, et al. , 2020. Detecting depression in people living with HIV in South Africa: the factor structure and convergent validity of the south African depression scale (SADS). AIDS Behav. 24 (8), 2282–2289. [PubMed: 31965430]

Arab T, Raffo-Romero A, Van Camp C, Lemaire Q, Le Marrec-Croq F, Drago F, et al. , 2019. Proteomic characterisation of leech microglia extracellular vesicles (EVs): comparison between differential ultracentrifugation and Optiprep density gradient isolation. J. Extracell. Ves 8 (1), 1603048.

Arab T, Mallick ER, Huang Y, Dong L, Liao Z, Zhao Z, et al. , 2021. Characterization of extracellular vesicles and synthetic nanoparticles with four orthogonal single-particle analysis platforms. J. Extracell. Ves 10 (6), e12079.

Bandaru VV, McArthur JC, Sacktor N, Cutler RG, Knapp EL, Mattson MP, et al. , 2007. Associative and predictive biomarkers of dementia in HIV-1-infected patients. Neurology. 68 (18), 1481–1487. [PubMed: 17470750]

Benjamin L, Khoo S, 2018. HIV infection and stroke. Handb. Clin. Neurol 152, 187–200. [PubMed: 29604976]

Berger JR, Avison M, 2004. The blood brain barrier in HIV infection. Front. Biosci 9, 2680–2685. [PubMed: 15358591]

Bertrand L, Meroth F, Tournebize M, Leda AR, Sun E, Toborek M, 2019. Targeting the HIV-infected brain to improve ischemic stroke outcome. Nat. Commun 10 (1), 2009. [PubMed: 31043599]

Bligh EG, Dyer WJ, 1959. A rapid method of total lipid extraction and purification. Can. J. Biochem. Physiol 37 (8), 911–917. [PubMed: 13671378]

Bocchio-Chiavetto L, Maffioletti E, Bettinsoli P, Giovannini C, Bignotti S, Tardito D, et al. , 2013. Blood microRNA changes in depressed patients during antidepressant treatment. Eur. Neuropsychopharmacol 23 (7), 602–611. [PubMed: 22925464]

Brown DA, London E, 2000. Structure and function of sphingolipid- and cholesterolrich membrane rafts. J. Biol. Chem 275 (23), 17221–17224. [PubMed: 10770957]

Brunkhorst-Kanaan N, Klatt-Schreiner K, Hackel J, Schroter K, Trautmann S, Hahnefeld L, et al. , 2019. Targeted lipidomics reveal derangement of ceramides in major depression and bipolar disorder. Metabolism. 95, 65–76. [PubMed: 30954559]

Cheng Y, Sun M, Chen L, Li Y, Lin L, Yao B, et al. , 2018. Ten-eleven translocation proteins modulate the response to environmental stress in mice. Cell Rep. 25 (11), 3194–203 e4. [PubMed: 30540950]

Cho HJ, Kuo AM, Bertrand L, Toborek M, 2017. HIV alters gap junction-mediated intercellular communication in human brain Pericytes. Front. Mol. Neurosci 10, 410. [PubMed: 29311803]

Ciesla JA, Roberts JE, 2001. Meta-analysis of the relationship between HIV infection and risk for depressive disorders. Am. J. Psychiatry 158 (5), 725–730. [PubMed: 11329393]

Consortium E-T, Van Deun J, Mestdagh P, Agostinis P, Akay O, Anand S, et al. , 2017. EV-TRACK: transparent reporting and centralizing knowledge in extracellular vesicle research. Nat. Methods 14 (3), 228–232. [PubMed: 28245209]

Crescitelli R, Lasser C, Jang SC, Cvjetkovic A, Malmhall C, Karimi N, et al. , 2020. Subpopulations of extracellular vesicles from human metastatic melanoma tissue identified by quantitative proteomics after optimized isolation. J. Extracell. Ves 9 (1), 1722433.

Denisova NA, Fisher D, Provost M, Joseph JA, 1999. The role of glutathione, membrane sphingomyelin, and its metabolites in oxidative stress-induced calcium "dysregulation" in PC12 cells. Free Radic. Biol. Med 27 (11–12), 1292–1301. [PubMed: 10641723]

Dickens AM, Yoo SW, Chin AC, Xu J, Johnson TP, Trout AL, et al. , 2017. Chronic low-level expression of HIV-1 tat promotes a neurodegenerative phenotype with aging. Sci. Rep 7 (1), 7748. [PubMed: 28798382]

Dinoff A, Herrmann N, Lanctot KL, 2017. Ceramides and depression: a systematic review. J. Affect. Disord 213, 35–43. [PubMed: 28189963]

Doyle K, Weber E, Atkinson JH, Grant I, Woods SP, Group HIVNRP, 2012. Aging, prospective memory, and health-related quality of life in HIV infection. AIDS Behav. 16 (8), 2309–2318. [PubMed: 22246512]

Du Y, Chi X, An W, 2019. Downregulation of microRNA-200c-3p reduces damage of hippocampal neurons in epileptic rats by upregulating expression of RECK and inactivating the AKT signaling pathway. Chem. Biol. Interact 307, 223–233. [PubMed: 31018114]

Dwivedi Y, Roy B, Lugli G, Rizavi H, Zhang H, Smalheiser NR, 2015. Chronic corticosterone-mediated dysregulation of microRNA network in prefrontal cortex of rats: relevance to depression pathophysiology. Transl. Psychiatry 5, e682. [PubMed: 26575223]

Emmanouilidou E, Melachroinou K, Roumeliotis T, Garbis SD, Ntzouni M, Margaritis LH, et al. , 2010. Cell-produced alpha-synuclein is secreted in a calcium-dependent manner by exosomes and impacts neuronal survival. J. Neurosci 30 (20), 6838–6851. [PubMed: 20484626]

Fan Y, Gao X, Chen J, Liu Y, He JJ, 2016. HIV tat impairs neurogenesis through functioning as a notch ligand and activation of notch signaling pathway. J. Neurosci 36 (44), 11362–11373. [PubMed: 27807176]

Fellows RP, Byrd DA, Morgello S, 2014. Effects of information processing speed on learning, memory, and executive functioning in people living with HIV/AIDS. J. Clin. Exp. Neuropsychol 36 (8), 806–817. [PubMed: 25111120]

Ferrarese C, Aliprandi A, Tremolizzo L, Stanzani L, De Micheli A, Dolara A, et al. , 2001. Increased glutamate in CSF and plasma of patients with HIV dementia. Neurology. 57 (4), 671–675. [PubMed: 11524477]

Fitzgerald PJ, Yen JY, Watson BO, 2019. Stress-sensitive antidepressant-like effects of ketamine in the mouse forced swim test. PLoS One 14 (4), e0215554. [PubMed: 30986274]

Ghosn J, Taiwo B, Seedat S, Autran B, Katlama C, 2018. Hiv. Lancet 392 (10148), 685–697. [PubMed: 30049419]

Giannessi F, Aiello A, Franchi F, Percario ZA, Affabris E, 2020. The role of extracellular vesicles as allies of HIV, HCV and SARS viruses. Viruses. 12 (5).

Gu CJ, Borjabad A, Hadas E, Kelschenbach J, Kim BH, Chao W, et al. , 2018. EcoHIV infection of mice establishes latent viral reservoirs in T cells and active viral reservoirs in macrophages that are sufficient for induction of neurocognitive impairment. PLoS Pathog. 14 (6), e1007061. [PubMed: 29879225]

Guha D, Lorenz DR, Misra V, Chettimada S, Morgello S, Gabuzda D, 2019. Proteomic analysis of cerebrospinal fluid extracellular vesicles reveals synaptic injury, inflammation, and stress response markers in HIV patients with cognitive impairment. J. Neuroinflammation 16 (1), 254. [PubMed: 31805958]

Gulbins E, Palmada M, Reichel M, Luth A, Bohmer C, Amato D, et al. , 2013. Acid sphingomyelinase-ceramide system mediates effects of antidepressant drugs. Nat. Med 19 (7), 934–938. [PubMed: 23770692]

Gulbins A, Grassme H, Hoehn R, Wilker B, Soddemann M, Kohnen M, et al. , 2016. Regulation of neuronal stem cell proliferation in the Hippocampus by endothelial ceramide. Cell. Physiol. Biochem 39 (2), 790–801. [PubMed: 27475812]

Hadas E, Borjabad A, Chao W, Saini M, Ichiyama K, Potash MJ, et al. , 2007. Testing antiretroviral drug efficacy in conventional mice infected with chimeric HIV-1. AIDS. 21 (8), 905–909. [PubMed: 17457083]

Hannun YA, 1996. Functions of ceramide in coordinating cellular responses to stress. Science. 274 (5294), 1855–1859. [PubMed: 8943189]

Haughey NJ, Cutler RG, Tamara A, McArthur JC, Vargas DL, Pardo CA, et al. , 2004. Perturbation of sphingolipid metabolism and ceramide production in HIV-dementia. Ann. Neurol 55 (2), 257–267. [PubMed: 14755730]

Haughey NJ, Steiner J, Nath A, McArthur JC, Sacktor N, Pardo C, et al. , 2008. Converging roles for sphingolipids and cell stress in the progression of neuro-AIDS. Front. Biosci 13, 5120–5130. [PubMed: 18508574]

He H, Sharer LR, Chao W, Gu CJ, Borjabad A, Hadas E, et al. , 2014. Enhanced human immunodeficiency virus type 1 expression and neuropathogenesis in knockout mice lacking type I interferon responses. J. Neuropathol. Exp. Neurol 73 (1), 59–71. [PubMed: 24335529]

Herbrich SM, Cole RN, West KP Jr., Schulze K, Yager JD, Groopman JD, et al. , 2013. Statistical inference from multiple iTRAQ experiments without using common reference standards. J. Proteome Res 12 (2), 594–604. [PubMed: 23270375]

Huang Y, Cheng L, Turchinovich A, Mahairaki V, Troncoso JC, Pletnikova O, et al. , 2020. Influence of species and processing parameters on recovery and content of brain tissue-derived extracellular vesicles. J. Extracell. Ves 9 (1), 1785746.

Ipinmoroti AO, Matthews QL, 2020. Extracellular vesicles: roles in human viral infections, immune-diagnostic, and therapeutic applications. Pathogens 9 (12).

Irie F, Hirabayashi Y, 1998. Application of exogenous ceramide to cultured rat spinal motoneurons promotes survival or death by regulation of apoptosis depending on its concentrations. J. Neurosci. Res 54 (4), 475–485. [PubMed: 9822158]

Abstracts of the 16th International Symposium on NeuroVirology November 12–16, 2019 Atlanta, GA, USA. J. Neuro-Oncol, 2019 1–51.

Jones LD, Jackson JW, Maggirwar SB, 2016. Modeling HIV-1 induced neuroinflammation in mice: role of platelets in mediating blood-brain barrier dysfunction. PLoS One 11 (3), e0151702. [PubMed: 26986758]

Kao CF, Chen HW, Chen HC, Yang JH, Huang MC, Chiu YH, et al. , 2016. Identification of susceptible loci and enriched pathways for bipolar II disorder using genome-wide association studies. Int. J. Neuropsychopharmacol 19 (12).

Kelschenbach JL, Saini M, Hadas E, Gu CJ, Chao W, Bentsman G, et al. , 2012. Mice chronically infected with chimeric HIV resist peripheral and brain superinfection: a model of protective immunity to HIV. J. NeuroImmune Pharmacol 7 (2), 380–387. [PubMed: 21987348]

Kelschenbach J, He H, Kim BH, Borjabad A, Gu CJ, Chao W, et al. , 2019. Efficient expression of HIV in immunocompetent mouse brain reveals a novel nonneurotoxic viral function in hippocampal Synaptodendritic injury and memory impairment. mBio. 10 (4).

Kim BH, Kelschenbach J, Borjabad A, Hadas E, He H, Potash MJ, et al. , 2019. Intranasal insulin therapy reverses hippocampal dendritic injury and cognitive impairment in a model of HIV-associated neurocognitive disorders in EcoHIV-infected mice. AIDS. 33 (6), 973–984. [PubMed: 30946151]

Lennox AL, Hoye ML, Jiang R, Johnson-Kerner BL, Suit LA, Venkataramanan S, et al. , 2020. Pathogenic DDX3X mutations impair RNA metabolism and neurogenesis during fetal cortical development. Neuron. 106 (3), 404–20 e8. [PubMed: 32135084]

Lopez-Montero I, Velez M, Devaux PF, 2007. Surface tension induced by sphingomyelin to ceramide conversion in lipid membranes. Biochim. Biophys. Acta 1768 (3), 553–561. [PubMed: 17292325]

Love MI, Huber W, Anders S, 2014. Moderated estimation of fold change and dispersion for RNA-seq data with DESeq2. Genome Biol. 15 (12), 550. [PubMed: 25516281]

Marquine MJ, Flores I, Kamat R, Johnson N, Umlauf A, Letendre S, et al. , 2018. A composite of multisystem injury and neurocognitive impairment in HIV infection: association with everyday functioning. J. Neuro-Oncol 24 (5), 549–556.

Martins-de-Souza D, Guest PC, Harris LW, Vanattou-Saifoudine N, Webster MJ, Rahmoune H, et al. , 2012. Identification of proteomic signatures associated with depression and psychotic depression in post-mortem brains from major depression patients. Transl. Psychiatry 2, e87. [PubMed: 22832852]

Masliah E, Heaton RK, Marcotte TD, Ellis RJ, Wiley CA, Mallory M, et al. , 1997. Dendritic injury is a pathological substrate for human immunodeficiency virus-related cognitive disorders. HNRC group. The HIV neurobehavioral research center. Ann. Neurol 42 (6), 963–972. [PubMed: 9403489]

Meerson A, Cacheaux L, Goosens KA, Sapolsky RM, Soreq H, Kaufer D, 2010. Changes in brain MicroRNAs contribute to cholinergic stress reactions. J. Mol. Neurosci 40 (1–2), 47–55. [PubMed: 19711202]

Michaelsen K, Murk K, Zagrebelsky M, Dreznjak A, Jockusch BM, Rothkegel M, et al. , 2010. Fine-tuning of neuronal architecture requires two profilin isoforms. Proc. Natl. Acad. Sci. U. S. A 107 (36), 15780–15785. [PubMed: 20798032]

Mielke MM, Bandaru VV, McArthur JC, Chu M, Haughey NJ, 2010. Disturbance in cerebral spinal fluid sphingolipid content is associated with memory impairment in subjects infected with the human immunodeficiency virus. J. Neuro-Oncol 16 (6), 445–456.

Muhle C, Wagner CJ, Farber K, Richter-Schmidinger T, Gulbins E, Lenz B, et al. , 2019. Secretory acid sphingomyelinase in the serum of medicated patients predicts the prospective course of depression. J. Clin. Med 8 (6).

Mukhamedova N, Hoang A, Dragoljevic D, Dubrovsky L, Pushkarsky T, Low H, et al. , 2019. Exosomes containing HIV protein Nef reorganize lipid rafts potentiating inflammatory response in bystander cells. PLoS Pathog. 15 (7), e1007907. [PubMed: 31344124]

Nanni MG, Caruso R, Mitchell AJ, Meggiolaro E, Grassi L, 2015. Depression in HIV infected patients: a review. Curr. Psychiatry Rep 17 (1), 530. [PubMed: 25413636]

Nedelcovych MT, Tenora L, Kim BH, Kelschenbach J, Chao W, Hadas E, et al. , 2017. N-(Pivaloyloxy)alkoxy-carbonyl prodrugs of the glutamine antagonist 6-Diazo-5-oxo-l-norleucine (DON) as a potential treatment for HIV associated neurocognitive disorders. J. Med. Chem 60 (16), 7186–7198. [PubMed: 28759224]

Nedelcovych MT, Kim BH, Zhu X, Lovell LE, Manning AA, Kelschenbach J, et al. , 2019. Glutamine antagonist JHU083 normalizes aberrant glutamate production and cognitive deficits in the EcoHIV murine model of HIV-associated neurocognitive disorders. J. NeuroImmune Pharmacol 14 (3), 391–400. [PubMed: 31209775]

Nickoloff-Bybel EA, Calderon TM, Gaskill PJ, Berman JW, 2020. HIV neuropathogenesis in the presence of a disrupted dopamine system. J. NeuroImmune Pharmacol 15 (4), 729–742. [PubMed: 32506353]

Niwa M, Kamiya A, Murai R, Kubo K, Gruber AJ, Tomita K, et al. , 2010. Knockdown of DISC1 by in utero gene transfer disturbs postnatal dopaminergic maturation in the frontal cortex and leads to adult behavioral deficits. Neuron. 65 (4), 480–489. [PubMed: 20188653]

Nowak JS, Michlewski G, 2013. miRNAs in development and pathogenesis of the nervous system. Biochem. Soc. Trans 41 (4), 815–820. [PubMed: 23863137]

Olson KE, Bade AN, Namminga KL, Potash MJ, Mosley RL, Poluektova LY, et al. , 2018. Persistent EcoHIV infection induces nigral degeneration in 1-methyl-4-phenyl-1,2,3,6-tetrahydropyridine-intoxicated mice. J. Neuro-Oncol 24 (4), 398–410.

Petrone A, Battaglia F, Wang C, Dusa A, Su J, Zagzag D, et al. , 2003. Receptor protein tyrosine phosphatase alpha is essential for hippocampal neuronal migration and long-term potentiation. EMBO J. 22 (16), 4121–4131. [PubMed: 12912911]

Potash MJ, Chao W, Bentsman G, Paris N, Saini M, Nitkiewicz J, et al. , 2005. A mouse model for study of systemic HIV-1 infection, antiviral immune responses, and neuroinvasiveness. Proc. Natl. Acad. Sci. U. S. A 102 (10), 3760–3765. [PubMed: 15728729]

Pulliam L, Sun B, Mustapic M, Chawla S, Kapogiannis D, 2019. Plasma neuronal exosomes serve as biomarkers of cognitive impairment in HIV infection and Alzheimer's disease. J. Neuro-Oncol 25 (5), 702–709.

Pyne S, Pyne NJ, 2000. Sphingosine 1-phosphate signalling in mammalian cells. Biochem. J 349 (Pt 2), 385–402. [PubMed: 10880336]

Rivera-Rivera Y, Vazquez-Santiago FJ, Albino E, Sanchez MD, Rivera-Amill V, 2016. Impact of depression and inflammation on the progression of HIV disease. J. Clin. Cell Immunol 7 (3).

Roberts A, Pachter L, 2013. Streaming fragment assignment for real-time analysis of sequencing experiments. Nat. Methods 10 (1), 71–73. [PubMed: 23160280]

Rojas C, Barnaeva E, Thomas AG, Hu X, Southall N, Marugan J, et al. , 2018. DPTIP, a newly identified potent brain penetrant neutral sphingomyelinase 2 inhibitor, regulates astrocyte-peripheral immune communication following brain inflammation. Sci. Rep 8 (1), 17715. [PubMed: 30531925]

Rojas C, Sala M, Thomas AG, Datta Chaudhuri A, Yoo SW, Li Z, et al. , 2019. A novel and potent brain penetrant inhibitor of extracellular vesicle release. Br. J. Pharmacol 176 (19), 3857–3870. [PubMed: 31273753]

Sa MJ, Madeira MD, Ruela C, Volk B, Mota-Miranda A, Paula-Barbosa MM, 2004. Dendritic changes in the hippocampal formation of AIDS patients: a quantitative Golgi study. Acta Neuropathol. 107 (2), 97–110. [PubMed: 14605830]

Saeedi S, Israel S, Nagy C, Turecki G, 2019. The emerging role of exosomes in mental disorders. Transl. Psychiatry 9 (1), 122. [PubMed: 30923321]

Sala M, Hollinger KR, Thomas AG, Dash RP, Tallon C, Veeravalli V, et al. , 2020. Novel human neutral sphingomyelinase 2 inhibitors as potential therapeutics for Alzheimer's disease. J. Med. Chem 63 (11), 6028–6056. [PubMed: 32298582]

Saman S, Kim W, Raya M, Visnick Y, Miro S, Saman S, et al. , 2012. Exosome-associated tau is secreted in tauopathy models and is selectively phosphorylated in cerebrospinal fluid in early Alzheimer disease. J. Biol. Chem 287 (6), 3842–3849. [PubMed: 22057275]

Satyanarayanan SK, Shih YH, Wen YR, Palani M, Lin YW, Su H, et al. , 2019. miR-200a-3p modulates gene expression in comorbid pain and depression: molecular implication for central sensitization. Brain Behav. Immun 82, 230–238. [PubMed: 31479730]

Saylor D, Dickens AM, Sacktor N, Haughey N, Slusher B, Pletnikov M, et al. , 2016. HIV-associated neurocognitive disorder–pathogenesis and prospects for treatment. Nat. Rev. Neurol 12 (4), 234–248. [PubMed: 26965674]

Shimizu SM, Chow DC, Valcour V, Masaki K, Nakamoto B, Kallianpur KJ, et al. , 2011. The impact of depressive symptoms on neuropsychological performance tests in HIV-infected individuals: a study of the Hawaii aging with HIV cohort. World J. AIDS 1 (4), 139–145. [PubMed: 23061029]

Skowronska M, McDonald M, Velichkovska M, Leda AR, Park M, Toborek M, 2018. Methamphetamine increases HIV infectivity in neural progenitor cells. J. Biol. Chem 293 (1), 296–311. [PubMed: 29158267]

Snyder JS, Soumier A, Brewer M, Pickel J, Cameron HA, 2011. Adult hippocampal neurogenesis buffers stress responses and depressive behaviour. Nature. 476 (7361), 458–461. [PubMed: 21814201]

Sun X, Song Z, Si Y, Wang JH, 2018. microRNA and mRNA profiles in ventral tegmental area relevant to stress-induced depression and resilience. Prog. NeuroPsychopharmacol. Biol. Psychiatry 86, 150–165. [PubMed: 29864451]

Tabatadze N, Savonenko A, Song H, Bandaru VV, Chu M, Haughey NJ, 2010. Inhibition of neutral sphingomyelinase-2 perturbs brain sphingolipid balance and spatial memory in mice. J. Neurosci. Res 88 (13), 2940–2951. [PubMed: 20629193]

Taibi DM, 2013. Sleep disturbances in persons living with HIV. J. Assoc. Nurses AIDS Care 24 (1 Suppl), S72–S85. [PubMed: 23290379]

Tallon C, Hollinger KR, Pal A, Bell BJ, Rais R, Tsukamoto T, et al. , 2021. Nipping disease in the bud: nSMase2 inhibitors as therapeutics in extracellular vesicle-mediated diseases. Drug Discov. Today 26 (7), 1656–1668. [PubMed: 33798648]

Tan LH, Tan AJ, Ng YY, Chua JJ, Chew WS, Muralidharan S, et al. , 2018. Enriched expression of neutral sphingomyelinase 2 in the striatum is essential for regulation of lipid raft content and motor coordination. Mol. Neurobiol 55 (7), 5741–5756. [PubMed: 29043558]

Tavazzi E, Morrison D, Sullivan P, Morgello S, Fischer T, 2014. Brain inflammation is a common feature of HIV-infected patients without HIV encephalitis or productive brain infection. Curr. HIV Res 12 (2), 97–110. [PubMed: 24862332]

Thaler NS, Sayegh P, Arentoft A, Thames AD, Castellon SA, Hinkin CH, 2015. Increased neurocognitive intra-individual variability is associated with declines in medication adherence in HIV-infected adults. Neuropsychology. 29 (6), 919–925. [PubMed: 25730729]

Thery C, Witwer KW, Aikawa E, Alcaraz MJ, Anderson JD, Andriantsitohaina R, et al. , 2018. Minimal information for studies of extracellular vesicles 2018 (MISEV2018): a position statement of the International Society for Extracellular Vesicles and update of the MISEV2014 guidelines. J. Extracell. Ves 7 (1), 1535750.

Tozzi V, Balestra P, Galgani S, Murri R, Bellagamba R, Narciso P, et al. , 2003. Neurocognitive performance and quality of life in patients with HIV infection. AIDS Res. Hum. Retrovir 19 (8), 643–652. [PubMed: 13678465]

Trajkovic K, Hsu C, Chiantia S, Rajendran L, Wenzel D, Wieland F, et al. , 2008. Ceramide triggers budding of exosome vesicles into multivesicular endosomes. Science 319 (5867), 1244–1247. [PubMed: 18309083]

Uthman OA, Magidson JF, Safren SA, Nachega JB, 2014. Depression and adherence to antiretroviral therapy in low-, middle- and high-income countries: a systematic review and meta-analysis. Curr. HIV/AIDS Rep 11 (3), 291–307. [PubMed: 25038748]

Valadi H, Ekstrom K, Bossios A, Sjostrand M, Lee JJ, Lotvall JO, 2007. Exoso-memediated transfer of mRNAs and microRNAs is a novel mechanism of genetic exchange between cells. Nat. Cell Biol 9 (6), 654–659. [PubMed: 17486113]

Verhoeven JE, Revesz D, Epel ES, Lin J, Wolkowitz OM, Penninx BW, 2014. Major depressive disorder and accelerated cellular aging: results from a large psychiatric cohort study. Mol. Psychiatry 19 (8), 895–901. [PubMed: 24217256]

Videbech P, Ravnkilde B, 2004. Hippocampal volume and depression: a meta-analysis of MRI studies. Am. J. Psychiatry 161 (11), 1957–1966. [PubMed: 15514393]

Wallensten J, Nager A, Asberg M, Borg K, Beser A, Wilczek A, et al. , 2021. Leakage of astrocyte-derived extracellular vesicles in stress-induced exhaustion disorder: a cross-sectional study. Sci. Rep 11 (1), 2009. [PubMed: 33479350]

Wei ZX, Xie GJ, Mao X, Zou XP, Liao YJ, Liu QS, et al. , 2020. Exosomes from patients with major depression cause depressive-like behaviors in mice with involvement of miR-139-5p-regulated neurogenesis. Neuropsychopharmacology. 45 (6), 1050–1058. [PubMed: 31986519]

Williams ME, Naude PJW, van der Westhuizen FH, 2021. Proteomics and metabolomics of HIV-associated neurocognitive disorders: a systematic review. J. Neurochem 157 (3), 429–449. [PubMed: 33421125]

Witwer KW, Sarbanes SL, Liu J, Clements JE, 2011. A plasma microRNA signature of acute lentiviral infection: biomarkers of central nervous system disease. AIDS. 25 (17), 2057–2067. [PubMed: 21857495]

Xu H, Bae M, Tovar-y-Romo LB, Patel N, Bandaru VV, Pomerantz D, et al. , 2011. The human immunodeficiency virus coat protein gp120 promotes forward trafficking and surface clustering of NMDA receptors in membrane microdomains. J. Neurosci 31 (47), 17074–17090. [PubMed: 22114277]

Xu F, Yang J, Chen J, Wu Q, Gong W, Zhang J, et al. , 2015. Differential co-expression and regulation analyses reveal different mechanisms underlying major depressive disorder and subsyndromal symptomatic depression. BMC Bioinformatics 16, 112. [PubMed: 25880836]

Zhou M, Wang M, Wang X, Liu K, Wan Y, Li M, et al. , 2018. Abnormal expression of MicroRNAs induced by chronic unpredictable mild stress in rat hippocampal tissues. Mol. Neurobiol 55 (2), 917–935. [PubMed: 28083819]

Zhu X, Nedelcovych MT, Thomas AG, Hasegawa Y, Moreno-Megui A, Coomer W, et al. , 2019. JHU-083 selectively blocks glutaminase activity in brain CD11b(+) cells and prevents depression-associated behaviors induced by chronic social defeat stress. Neuropsychopharmacology. 44 (4), 683–694. [PubMed: 30127344]
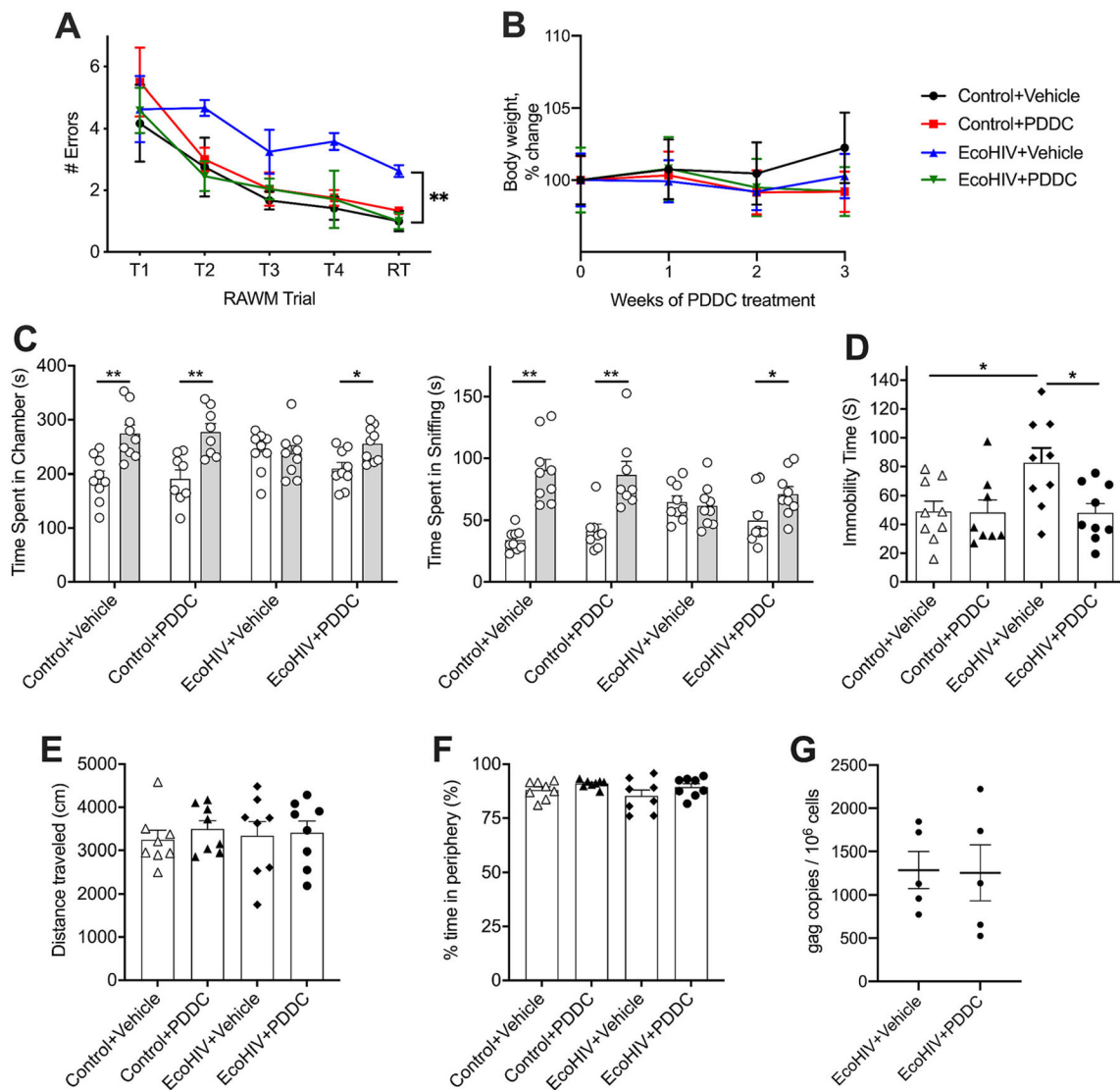
**Fig. 1.**
PDDC improves neurocognitive deficits and depressive-like behaviors in EcoHIV-infected mice. (A) Daily 30 mg/kg PDDC improved cognition in EcoHIV-infected mice as measured by number of errors made in the radial arm water maze. EcoHIV+Vehicle mice exhibited impairment versus Control+Vehicle mice. PDDC significantly reduced the numbers of errors within the EcoHIV cohort. Values are averages of the last 3 days of testing. (B) PDDC does not affect body weight in Control or EcoHIV-infected mice. (C and D) PDDC normalized depressive-like behaviors in EcoHIV-infected mice as measured by time spent in the chamber with and time sniffing a stranger mouse (grey bars) versus an inanimate toy (white bars) in the social interaction test (C) and immobility time in the forced swim test (D). (E and F) PDDC treatment impacts neither locomotion (E) nor anxiety behaviors reflected by percentage of time in periphery area (F) in the open field test in Control and EcoHIV-infected mice. (A-F) $n = 8–9$ in each group. Data represent mean ± SEM. *$P <$ 0.05, **$P <$ 0.01, by two-way ANOVA. (G) PDDC treatment does not alter splenic viral

burden as measured by gag DNA. $n = 5$ in each group. Data represent mean ± SEM. Analyzed by Student's *t*-test.
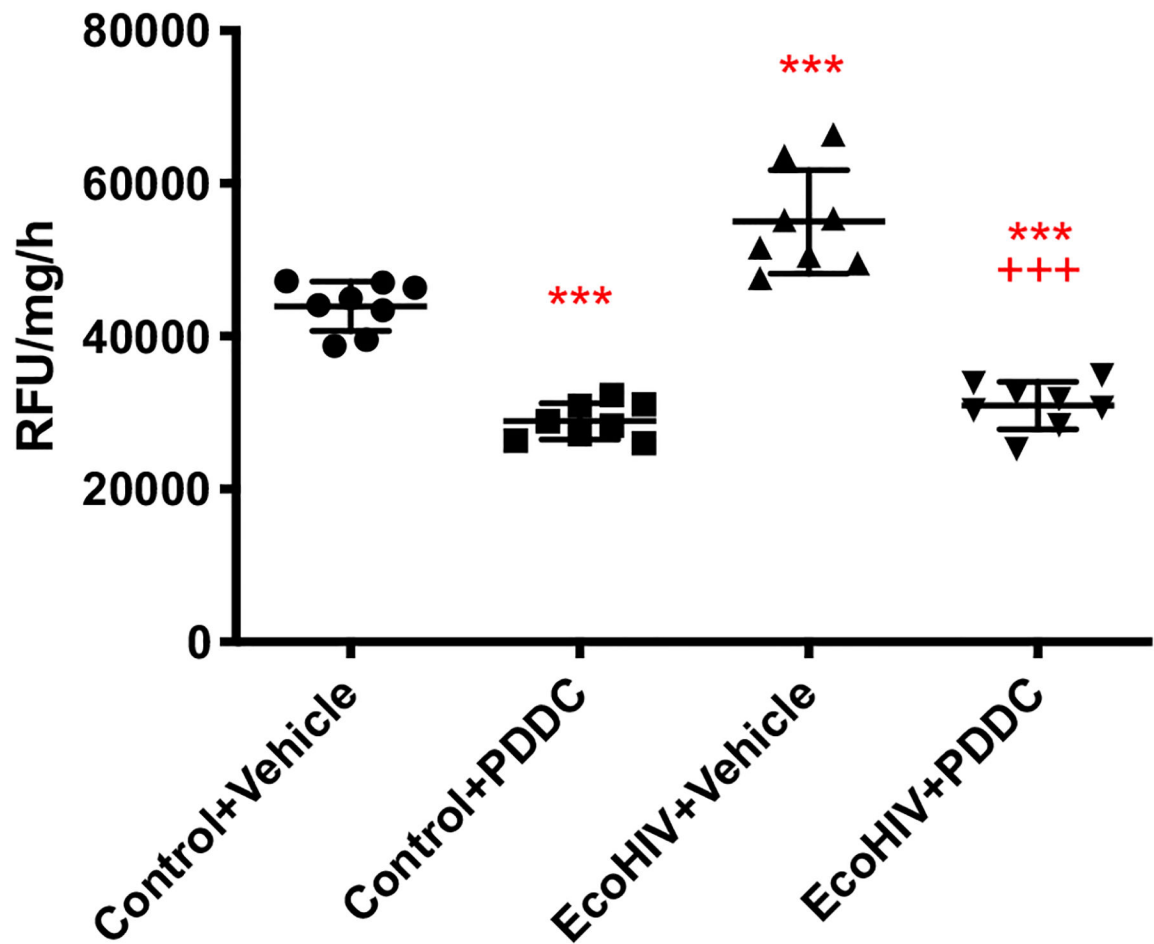
**Fig. 2.**
PDDC inhibits elevation of nSMase2 activity in EcoHIV-infected mice. Primary cortices from groups of mice were dissected and analyzed for nSMase2 activity. $n = 8$ in each group. Data represent mean ± SEM. ***$P < 0.001$, all other groups comparing with Control+Vehicle, +++$P < 0.001$, EcoHIV+PDDC comparing with EcoHIV+Vehicle, by two-way ANOVA.
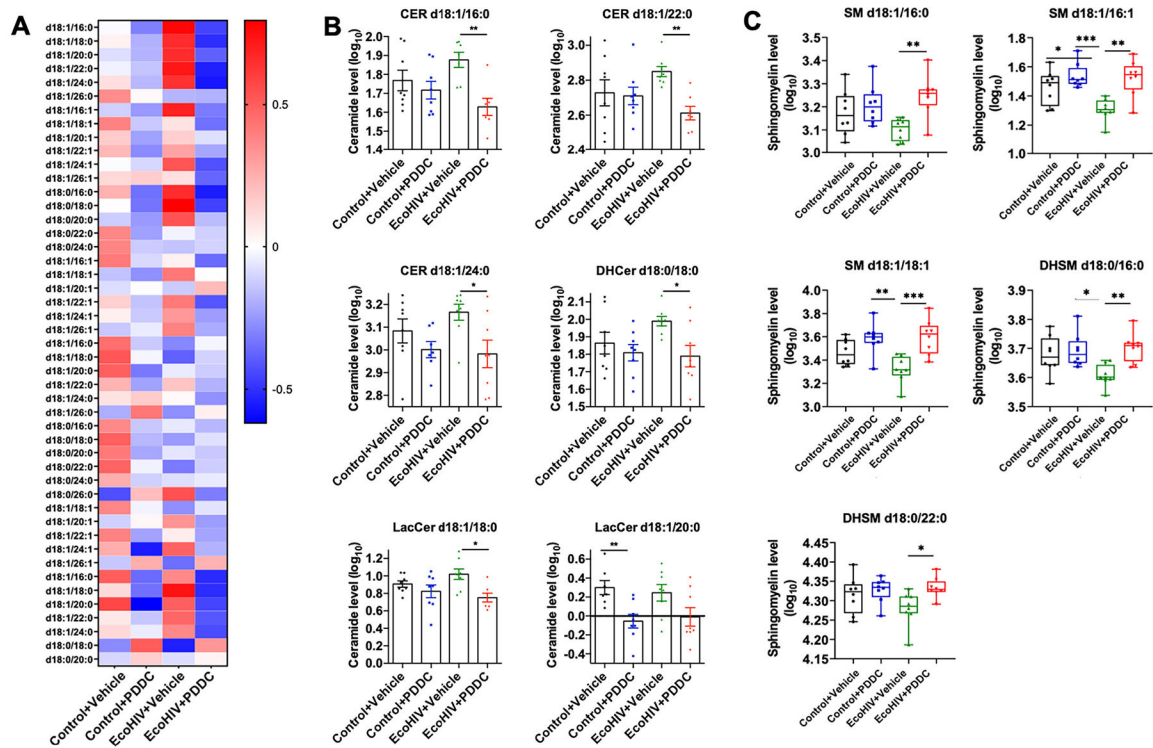
**Fig. 3.**
Cortical ceramide and sphingomyelin levels in PDDC-treated mice. Daily 30 mg/kg PDDC significantly altered levels of cortical ceramides and sphingo-myelins as measured by LC-ESI-MS/MS. PDDC reduced ceramide levels and increased sphingomyelin levels in EcoHIV mice. Ceramide and sphingomyelin concentrations were measured from cortical lipid extracts and calculated by fitting the identified individual species to these standard curves based on acyl chain length. (A-C) $Z$-score normalized data in heatmap showing the overall changes in ceramide levels (A), and individual changes in ceramide (B) and sphingomyelin levels (C) among the groups. (B and C) $n = 6$–8 in each group. Data represent mean ± SEM. *$P < 0.05$, **$P < 0.01$, by two-way ANOVA.
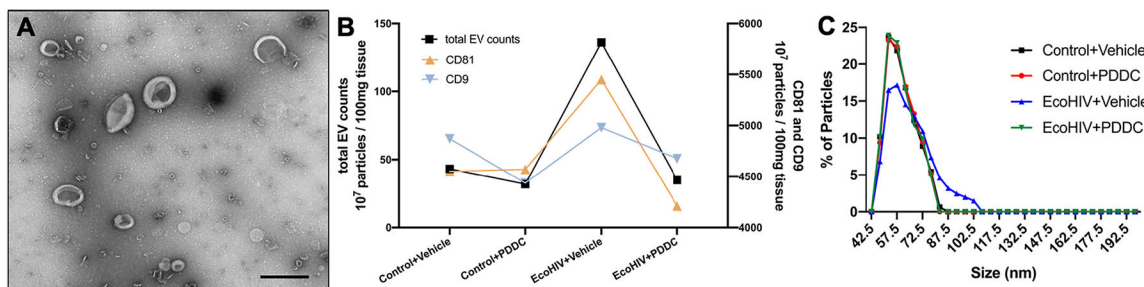
**Fig. 4.**
Brain-derived EV Characterization. (A) Sample transmission electron microscopy image of brain-derived EVs (bdEVs). Magnification = 50,000×, scale bar = 500 nM. (B) Brain-derived EV particle concentration were measured by nanoparticle flow cytometry and levels of the EV-associated markers CD81 and CD9 found in EV samples were measured by single particle interferometric reflectance imaging and normalized per 100 mg tissue. (C) Size distribution in bdEVs measured by Nano flow FCM analysis. Data represent samples pooled from 6 to 8 mice/group.
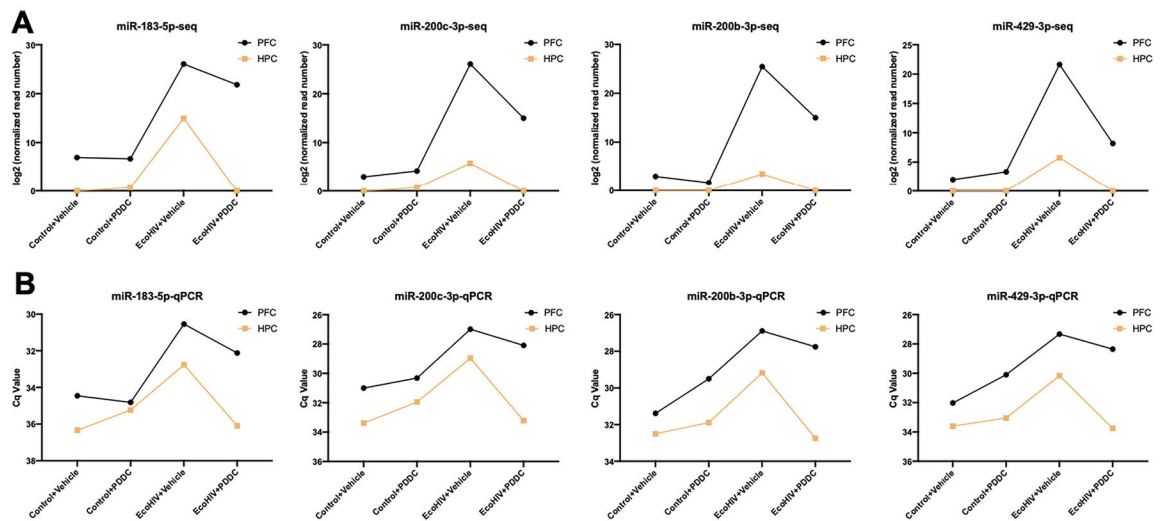
**Fig. 5.**

PDDC altered brain-derived EV miRNA content. EcoHIV upregulated expression of miR-183-5p, miR-200c-3p, miR-200b-3p, and miR-429-3p, miRNAs associated with cognitive impairment and major depressive disorder, in EVs isolated from prefrontal cortex and hippocampus as measured by (A) sequencing and (B) qPCR analyses. EcoHIV-mediated increases in miRNA levels were reduced by daily 30 mg/kg PDDC treatment. Small RNA libraries were constructed from RNA extracted from bdEVs and used for deep sequencing, and individual TaqMan miRNA qPCR assays were performed. Data represent samples pooled from 6 to 8 mice/group.

**Table 1**

Similarities between EcoHIV-infected rodents and PLH.

| Phenotypes | EcoHIV-Infected mice | PLH |
|---|---|---|
| Neurobehavioral Cognitive impairment | (Gu et al., 2018; Nedelcovych et al., 2017; Kelschenbach et al., 2019; Nedelcovych et al., 2019) | (Thaler et al., 2015; Marquine et al., 2018; Doyle et al., 2012; Tozzi et al., 2003; Saylor et al., 2016) |
| Depression | Present studies | (Ciesla and Roberts, 2001; Uthman et al., 2014; Anagnostopoulos et al., 2015) |
| Sleep abnormalities | (J. Neuro-Oncol., 2019) | (Taibi, 2013) |
| Physiological BBB disruption | (Jones et al., 2016; Cho et al., 2017) | (Berger and Avison, 2004) |
| Altered lipid metabolism | Present Studies | (Haughey et al., 2008; Saylor et al., 2016) |
| Neuroinflammation | (Kelschenbach et al., 2019; Potash et al., 2005; He et al., 2014; Jones et al., 2016) | (Tavazzi et al., 2014) |
| Elevated risk of ischemic stroke | (Bertrand et al., 2019) | (Benjamin and Khoo, 2018) |
| Increased glutamate levels | (Nedelcovych et al., 2019) | (Ferrarese et al., 2001) |
| Dopaminergic neuronal injury | (Olson et al., 2018) | (Nickoloff-Bybel et al., 2020) |
| Synaptodendritic injury | (Kelschenbach et al., 2019; Kim et al., 2019) | (Masliah et al., 1997; Sa et al., 2004) |
| cART-mediated viral suppression | (Gu et al., 2018) | (Ghosn et al., 2018) |